Integrated Isolated AC/DC Converter Using IOFL for LED Driver Applications

Behnam Vakili, Mitra Sarhangzadeh, Arez Nostratpour, and Jaber Fallah Ardashir

***Abstract*—Power factor correction, voltage and current ripple reduction, and eradicating short-life electrolytic capacitors are challenging issues in state-of-the-art ac/dc light-emitting-diode (LED) drivers. The conventional single-stage drivers need an electrolytic capacitor to ensure low output current flicker. However, electrolyte capacitors having a high failure rate reduce the lifespan of the LED driver. To cover these challenges, in this article, an integrated LED driver is proposed. The proposed driver is combined of three dc/dc converters with only one active switch. It features high-power factor and low-current flicker, and due to using only one active switch, its cost, volume, complexity, and power loss are low. The driver is analyzed step-by-step to show the operation principles based on the duty cycle variations. Dynamic analysis and control design of the proposed driver is presented based on the nonlinear control by input–output feedback linearization. The simulation and experimental results have been provided to verify the versatility of the proposed driver.**

***Index Terms*—Current ripple reduction, input–output feedback linearization (IOFL), integrated dc–dc converter, light-emitting diodes (LEDs), light flicker, steady-state analysis.**

I. Introduction

LIGHT-EMITTING diodes (LEDs) are semiconductor light source that release energy in the form of photons when directly biased. This effect is called electroluminescence. The color of light (proportional to the photon energy) is determined by the semiconductor energy gap. These devices emit light when exposing to an electric current, where the intensity of the light emitted directly depends on the value of the current passing through it. LEDs, alike diodes, need dc current and voltage to light up. The brightness of LEDs is adjusted by modulating the current passing through it. As the current passing through the LED increases, the emitted light increases.

Traditionally, to control the current of LEDs, resistance-based current limiters and linear regulators were employed [1]. Nowadays, the brightness of the LED is usually adjusted by using pulsewidth modulation switching strategy to control voltage or current of LEDs [1], [2], [3], [4].

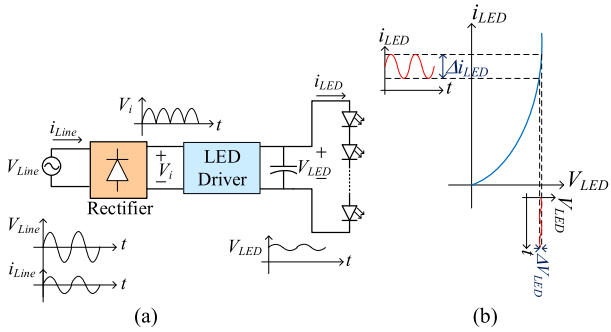

Fig. 1. (a) Overall schematic of LED driver. (b) Current and voltage changes in LED voltage/current characteristic.

A converter with a voltage controlling unit has a constant voltage and variable current, while power LEDs require a constant current. A converter with current controlling unit has a constant output current with variable voltage. Therefore, current converter, called LED driver, is used to drive LEDs. As a result, when using LED drivers, which are equipped with current controller, arbitrary number of LEDs can be connected in series [1], [2], [3]. Therefore, switching power sources, which consist voltage/current controlling units, can achieve high efficiency, high-power density, and precise control accuracy, making them ideal candidates for high-power LED drivers.

The main features of an ideal LED driver are to offer high-power factor and low harmonics at the ac side, low-current ripple and low-light flicker in LEDs, as well as electrolytic capacitorless with durable and long-life structure. Drivers with power factor correction (PFC) capability, which is called the PFC converters, and power controlling capability, which is called Power Controller (PC) converters, offer higher efficiency, desired output current, and appropriate harmonic standards [4], [5]. As shown in Fig. 1(a), the input voltage of the LED driver (V_i) is the output voltage of a rectifier. In order to have a unity power factor in ac side, there should be no capacitor in the rectifier output. The absence of a capacitor at the dc side of the rectifier causes high-voltage fluctuations at its output, which results in a nonsmooth dc-link voltage (V_i). Therefore, V_i comprises of dc and ac parts, where the frequency of its fundamental ac component is twice the frequency of the ac grid [5]. In other words, the input voltage fluctuates with double line frequency ripple [6]. The voltage ripple of V_i causes high voltage ripple

Manuscript received 6 December 2022; revised 29 January 2023 and 12 March 2023; accepted 10 April 2023. Date of publication 17 April 2023; date of current version 19 May 2023. This work was supported by Department of Electrical Engineering, Sanandaj Branch, Islamic Azad university, Sanandaj, Iran. Recommended for publication by Associate Editor X. Qu. *(Corresponding author: Mitra Sarhangzadeh.)*

Behnam Vakili and Arez Nostratpour are with the Department of Electrical Engineering, Sanandaj Branch, Islamic Azad University, Sanandaj, Iran (e-mail: behnam.vakili@iausdj.ac.ir; a.nosratpour@iausdj.ac.ir).

Mitra Sarhangzadeh and Jaber Fallah Ardashir are with the Department of Electrical Engineering, Tabriz Branch, Islamic Azad University, Tabriz, Iran (e-mail: mitsarhang@iaut.ac.ir; j.fallah@iaut.ac.ir).

Color versions of one or more figures in this article are available at https://doi.org/10.1109/TPEL.2023.3266796.

Digital Object Identifier 10.1109/TPEL.2023.3266796

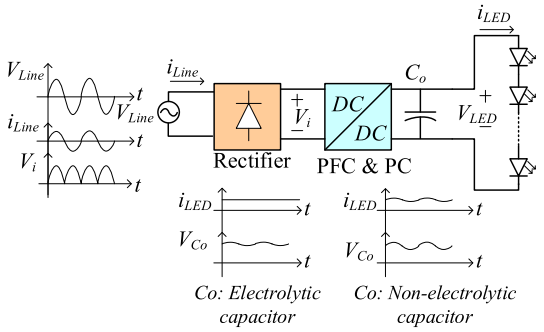

Fig. 2. Overall schematic of single-stage LED driver.

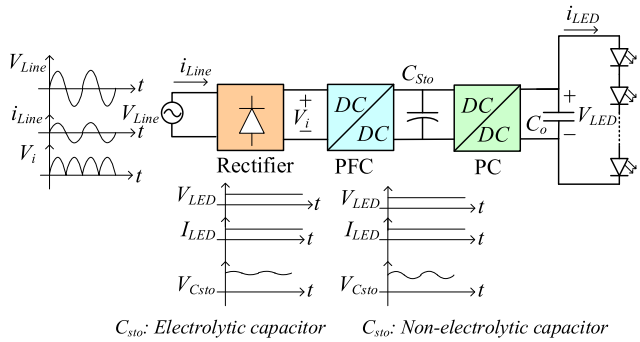

Fig. 3. Overall schematic of two-stage LED driver.

at the output side of the LED driver (ΔV_{LED}). As shown in Fig. 1(b), if the driver does not have a proper structure and controller, due to the nonlinearity of the LED voltage/current characteristic, a small ripple in the LED voltage causes a large ripple in the LED current (Δi_{LED}). A large current ripple in the LED causes light flicker [7], [8], [9]. To avoid the mentioned problems, many LED driver topologies have been introduced so far. In the conventional LED driver, to reduce voltage and current ripple in LED side, large capacitors are used in LED side. Considering that large capacitors are of electrolytic type and the lifespan of these types of capacitors is about 5000 h, and the expected lifespan of LEDs is about 50 000 h, the electrolytic capacitors can decrease the estimated lifespan of LED drivers [10]. In order to increase the expected lifetime of LED drivers, the electrolytic capacitor must be eliminated from the circuit. Therefore, to overcome this problem in single-stage drivers, two solutions can be resorted: first, increasing switching frequency, and second, using multistage converters. Increasing switching frequency causes extra power loss and necessitate using expensive and complicated high-frequency devices, for example GaN semiconductors.

Increasing the number of converting stages, however necessitate using high number of component, makes it possible to use low-capacitance nonelectrolyte capacitors without increasing switching frequency.

In multistage LED drivers, voltage ripple is reduced through several stages (two or three stages). To this end, each stage uses one low-capacitance nonelectrolyte capacitor. In other word, in multistage LED driver, each stage shoulders reducing a portion of voltage ripple by using small-size nonelectrolyte capacitors without increasing switching frequency and accordingly switching losses. While multistage LED drivers need many number of switching devices, the attempt is to approach to a multistage LED driver with minimum number of component. This can be achieved by integrating the stages. In this way, it is practical to use small ceramic or polyester types that have lower failure rate [11], [12], [13]. Therefore, LED drivers can be divided into integrated, single-stage, two-stage, and three-stage categories. Any of them can be single or multiple outputs. The single-stage driver, which is depicted in Fig. 2, has only one dc–dc converter as PFC and PC cell simultaneously. An electrolyte-capacitorless single-stage driver has a high-power factor at the input but a high ripple at the output. In these types of drivers, a large electrolytic capacitor can be used at the output to eliminate the current ripple; however, it comes at the cost of shortening the lifespan of the driver [14], [15], [16], [17].

To solve the problems of the single-stage drivers, two-stage and three-stage divers can be employed. Since each stage uses a capacitor, increasing the number of stages means using higher number of capacitors and reduced voltage and current ripple. At first glance, using higher number of capacitor seems as a drawback; however, the size of capacitor in each stages is reduced. Thus, it is possible to use small-size nonelectrolyte capacitors and reduced the ripple. Increasing the number of stages comes with the expense of using many switches causing increased complexity and cost. Therefore, the attempt is to increase the number of converting stages by employing fewer number of switches.

The overall structure of a two-stage driver is shown in Fig. 3. As shown in this figure, two-stage drivers are combined of two dc–dc converters, where the first converter is used to correct the power factor and the second converter is used to control the output current [11], [12], [13]. As it is observed in this figure, to approach to a smooth voltage and current at the output terminal of the driver, whether or not the output capacitor (C_{sto}) of PFC unit is electrolyte or not-electrolyte type, there is no need to use a large electrolyte capacitor (C_o) at the output side of the PC unit. Thus, to increase the lifespan of the LED driver, it would be better to use nonelectrolyte capacitor (C_{sto}) at the output side of the PFC unit as well.

The only drawback of two-stage drivers is using a large number of elements, which increases the cost, complexity, and volume. To address the mentioned problem, integrated drivers can be used. In principle, integrated drivers that include two or three stages use some common elements to reduce the utilized components and complexity [18], [19], [20], [21]. The overall structure of integrated LED drivers is demonstrated in Fig. 4. To sum up, an ideal driver offers a high-power factor, pure sinusoidal current on the ac side, smooth LED current, high efficiency, small size, low cost, and long lifespan.

In light of above, to eliminate electrolyte capacitor and increase the lifespan of the drivers used in LED application, a new integrated LED driver is proposed. The proposed LED driver in this article uses three dc–dc converters (buck, buck/boost, and

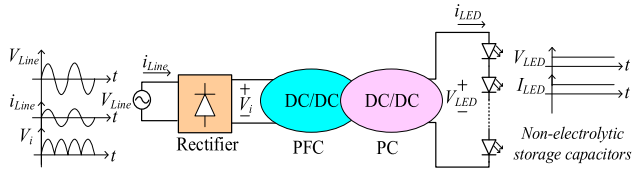

Fig. 4. Overall schematic of integrated LED driver.

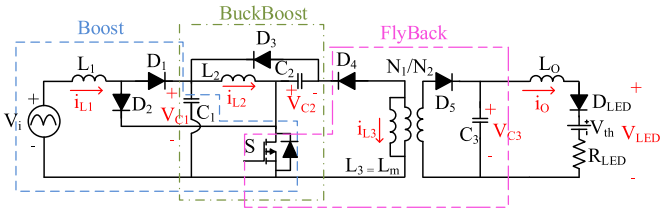

Fig. 5. Proposed integrated LED driver.

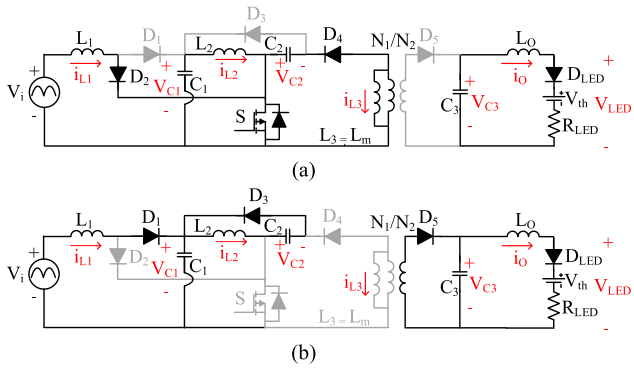

Fig. 6. Operating modes. (a) Mode I. (b) Mode II.

TABLE I
OPERATING MODES

Mode	Intervals	Description	Duration time (T_s)
1	t_0- t_1	S, D_2, D_4: ON	DT_s
2	t_1- t_2	D_1, D_3, D_5: ON	$(1-D)T_s$

flyback). The proposed LED driver uses three stages using one active switch and three small nonelectrolyte capacitors. By the three converting stages in the proposed driver, it is possible to correct the power factor at the ac side, adjust the voltage magnitude, and isolate the LEDs from the input side without increasing frequency and switching power loss. Furthermore, since all the three stages are handled by only one active switch, the cost and complexity are reduced in the proposed LED driver. The analysis of the proposed driver is carried out by providing simulation and experimental results. Furthermore, due to fast response, dynamic analysis and nonlinear controller based on input–output feedback linearization (IOFL) for the proposed LED driver is designed. The provided experimental results, which are obtained by employing a prototype, prove the theoretical analysis.

The rest of this article is organized as follows. In Section II, the proposed LED driver is modeled and analyzed. In Section III, the way to calculate output voltage ripple is described. In Section IV, the designed IOFL controller for the proposed driver is explained. The proposed driver is compared with the prior-art drivers in Section V. The simulation and experimental results are provided in Section VI to investigate the performance of the proposed driver and designed IOFL controller under different operation modes. Finally, Section VII concludes this article.

II. Modeling and Analysis of the Proposed LED Driver

Fig. 5 shows the configuration of the proposed integrated LED driver. As seen in this figure, the proposed driver is composed of a boost converter (PFC cell) integrated with a buck/boost and flyback converters (PC cell).

Since boost converter uses an input inductor (L_1), the input inductor in this converter acts as an input current filter. So, this converter mostly is used as a PFC unit. This is also the case in the proposed LED driver. The flyback in the proposed converter is used to isolate the LEDs from the input. Furthermore, through the transformer ratio of this converter, it is possible to reach to an arbitrary voltage magnitude. What is more, the buck–boost converter is used both to handle the voltage magnitude and increase the number of stages aiming at reducing the capacitor size and voltage ripple. In addition, this converter recovers the energy of the parasitic inductor of the transformer utilized in flyback converter.

The elements L_1, D_1, D_2, and C_1 synthesize the boost converter and L_2, D_3, and C_2 synthesize the buck–boost converter; the flyback converter consists of a transformer, two diodes D_4 and D_5, an output capacitor C_3, and inductor L_o. As an advantage, all of the mentioned converters share the same active switch (S). For clarity, in Fig. 4, the transformer is modeled by a magnetizing inductance $L_{\rm m} = L_3$ and an ideal transformer ratio of N_1/N_2. The input ac source along with the bridge diodes is substituted by a rectified sinusoidal voltage source (V_i), the LED is modeled with an ideal diode ($D_{\rm LED}$), resistance ($R_{\rm LED}$), and a voltage source ($V_{\rm th}$) in series.

In order to model the proposed LED driver, the following assumptions are considered.

All semiconductor devices are ideal.

The capacitors C_1, C_2, and C_3 are large enough in which the voltages across them are constant during switching frequency.

The switching frequency f_s is considerably higher than the line frequency ($f = 50$ Hz) so that the input voltage is constant during a switching interval (T_s).

Under steady-state condition, the proposed LED driver has two operating modes. Circuit diagram of these modes is depicted in Fig. 6. To illustrate the mentioned modes, a switching interval from t_0 to t_2 is considered, as shown in Fig. 7. This switching interval is divided into two operating modes, as listed in Table I, where, "D" indicates the duty cycle of S.

The main waveforms of the proposed driver during a switching period are illustrated in Fig. 7.

In this section, the proposed LED driver topology is modeled using the state-space modeling approach. Considering switching modes in Table I and operation modes in Figs. 6 and 7, the

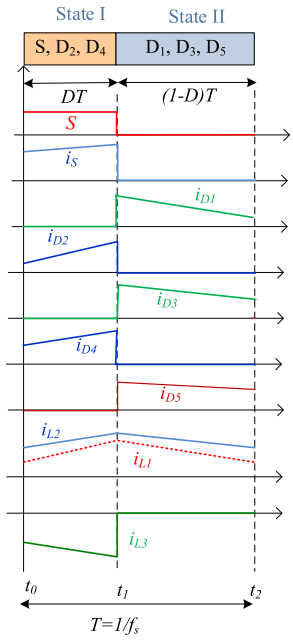

Fig. 7. Main waveforms during a given switching interval.

average steady space equations are presented by (1)–(3)

$$\begin{bmatrix} i'_{L_1} \\ i'_{L_2} \\ i'_{L_3} \\ V'_{C_1} \\ V'_{C_2} \\ V'_{C_3} \\ i'_o \end{bmatrix} = A \begin{bmatrix} i_{L_1} \\ i_{L_2} \\ i_{L_3} \\ V_{C_1} \\ V_{C_2} \\ V_{C3} \\ i_o \end{bmatrix} + B \begin{bmatrix} V_i \\ V_{\text{th}} \end{bmatrix} \tag{1}$$

where r_d and r_s are the ON-state resistance of each diode and switch, accordingly, and A and B are given as in (2) shown at the bottom of this page.

$$B = \begin{bmatrix} \frac{1}{L_1} & 0 \\ 0 & 0 \\ 0 & 0 \\ 0 & 0 \\ 0 & 0 \\ 0 & 0 \\ 0 & -\frac{1}{L_o} \end{bmatrix}. \tag{3}$$

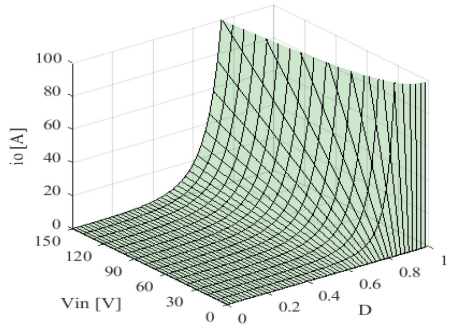

Fig. 8. Variations of output current (i_o) versus duty cycle (D) and input voltage (V_i).

By ignoring the ON-state resistance of diodes and switch, the dc part of steady-state equation can be written as follows:

$$x_{\text{dc}} = \begin{bmatrix} i_{L_1} \\ i_{L_2} \\ i_{L_3} \\ V_{C1} \\ V_{C2} \\ V_{C3} \\ i_o \end{bmatrix} = \begin{bmatrix} \left(\frac{N_2}{N_1}\right)^2 \frac{D^4 Vi}{(1-D)^6 R_{\text{LED}}} + \frac{N_2}{N_1} \frac{D^2 V_{\text{th}}}{(D-1)^3 R_{\text{LED}}} \\ \left(\frac{N_2}{N_1}\right)^2 \frac{D^3 Vi}{(1-D)^5 R_{\text{LED}}} - \frac{N_2}{N_1} \frac{DV_{\text{th}}}{(D-1)^2 R_{\text{LED}}} \\ -\left(\frac{N_2}{N_1}\right)^2 \frac{D^2 Vi}{(1-D)^4 R_{\text{LED}}} - \frac{N_2}{N_1} \frac{V_{\text{th}}}{(D-1) R_{\text{LED}}} \\ \frac{V_i}{(1-D)} \\ \frac{DV_i}{(1-D)^2} \\ \frac{N_2}{N_1} \frac{D^2 Vi}{(1-D)^3} \\ \frac{N_2}{N_1} \frac{D^2 Vi}{(1-D)^3 R_{\text{LED}}} - \frac{V_{\text{th}}}{R_{\text{LED}}} \end{bmatrix}. \tag{4}$$

The last row of (4) presents the relation between i_o, V_i, and D. Fig. 8 depicts the variation of the output current against D and input voltage V_i.

One of the important parameters in the competency of the power electronic devices is voltage stress of the components. This parameter for the utilized diodes and switches in the proposed LED driver is given as follows:

$$V_{\text{Stress}-D_1} = \frac{V_i}{(1-D)} \tag{5}$$

$$V_{\text{Stress}-D_2} = \frac{DV_i}{(1-D)^2} \tag{6}$$

$$V_{\text{Stress}-D_3} = \frac{V_i}{(1-D)^2} \tag{7}$$

$$A = \begin{bmatrix} \frac{-Dr_s - r_d}{L_1} & \frac{-Dr_s}{L_1} & \frac{Dr_s}{L_1} & \frac{D-1}{L_1} & 0 & 0 & 0 \\ \frac{-Dr_s}{L_2} & -\frac{r_d + (r_s - r_d)D}{L_2} & \frac{Dr_s}{L_2} & \frac{D}{L_2} & \frac{D-1}{L_2} & 0 & 0 \\ \frac{Dr_s}{L_3} & \frac{Dr_s}{L_3} & \frac{-Dr_s - r_d}{L_3} & 0 & \frac{-D}{L_3} & \frac{N_1}{N_2}\frac{1-D}{L_3} & 0 \\ \frac{1-D}{C_1} & \frac{-D}{C_1} & 0 & 0 & 0 & 0 & 0 \\ 0 & \frac{1-D}{C_2} & \frac{D}{C_2} & 0 & 0 & 0 & 0 \\ 0 & 0 & \frac{N_1}{N_2}\frac{D-1}{C_3} & 0 & 0 & 0 & \frac{-1}{C_3} \\ 0 & 0 & 0 & 0 & 0 & \frac{1}{L_o} & \frac{-R_{\text{LED}}}{L_o} \end{bmatrix} \tag{2}$$

$$V_{\text{Stress}-D_4} = \frac{(1-2D)\,V_i}{(1-D)^3} \tag{8}$$

$$V_{\text{Stress}-D_5} = \frac{N_2}{N_1}\frac{DV_i}{(1-D)^3} \tag{9}$$

$$V_{\text{Stress}-S} = \frac{(1-2D)\,V_i}{(1-D)^2}. \tag{10}$$

The size of the capacitors C_1, C_2, and C_3 can be calculated by referring to Mode1 in steady-state equations. For ease of reference, the equation to figure out the size of capacitors is given as follows:

$$C_1 = \frac{i_{L2}D}{f_s\Delta V_{C1}} \tag{11}$$

$$C_2 = \frac{i_{L3}D}{f_s\Delta V_{C2}} \tag{12}$$

$$C_3 = \frac{i_oD}{f_s\Delta V_{C3}}. \tag{13}$$

III. Output Voltage Ripple Calculation

Due to using full-bridge rectifier in the input side of the proposed LED driver, the voltage at this side is given as follows:

$$v_i\,(t) = V_m\,|\sin\,(\omega t)| \tag{14}$$

where $\omega = 2\pi f$ and f is the line frequency. Hence, the dc and ac components of V_i are

$$v_i\,(t) = V_{i\text{dc}} + \sum_{n=1}^{k} V_{\text{iac}-n}\sin\,(2\,n\,\omega\,t). \tag{15}$$

Therefore, the ac parts of V_i are as follows:

$$v_{i\text{ac}}\,(t) = \sum_{n=1}^{k} V_{\text{iac}-n}\sin\,(2\,n\,\omega\,t). \tag{16}$$

In order to calculate the ac ripple (double line frequency) effect on the output current ripple, assuming only the first ac component of the input voltage, the voltage and current ripples of different parts are figured out. For the ease of reference, the ac models of different parts of the proposed driver are exhibited in Fig. 9. In order to calculate the input ac current (i_{L1}) in boost part, the input impedance of the three parts of the proposed driver (shown in Fig. 9) should be obtained as follows:

$$Z_f = \frac{1}{\frac{D^2}{j\omega L_3} - \frac{\frac{D^2(1-D)^2}{j\omega L_3}}{\frac{1}{a^2R}+\frac{j\omega C_3}{a^2}+\frac{(1-D)^2}{j\omega L_3}}\left(\frac{1}{j\omega L_3}+\frac{1}{\frac{1}{a^2R}+\frac{j\omega C_3}{a^2}}\right)} \tag{17}$$

$$Z_{bb} = \frac{1}{\frac{D^2}{j\omega L_2} - \frac{\frac{D^2(1-D)^2}{j\omega L_2}}{\frac{1}{Z_f}+j\omega C_2+\frac{(1-D)^2}{j\omega L_2}}\left(\frac{1}{j\omega L_2}+\frac{1}{\frac{1}{Z_f}+j\omega C_2}\right)} \tag{18}$$

$$Z_b = \frac{1}{\frac{1}{j\omega L_1} + \frac{(1-D)^2}{\omega^2 L_1^2}\frac{1}{\frac{1}{Z_{bb}}+j\omega C_1+\frac{(1-D)^2}{j\omega L_1}}}. \tag{19}$$

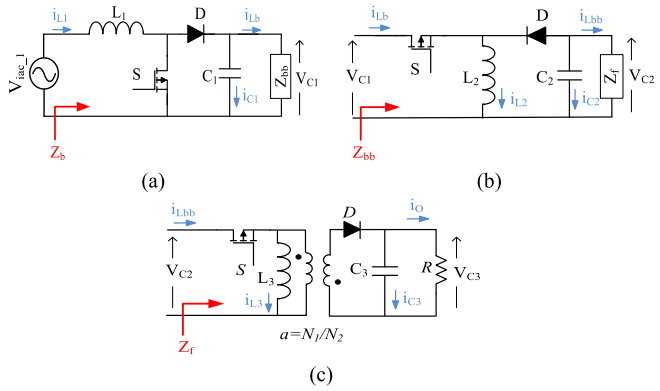

Fig. 9. AC model of different parts of the proposed driver and input impedances. (a) Boost, (b) buck–boost, and (c) flyback converters.

The input current is calculated as

$$i_{L1}(t) = \frac{v_{\text{iac}-1}(t)}{Z_b} = \frac{v_{\text{iac}-1}(t)-(1-D)v_{C1}(t)}{jL_1\omega}. \tag{20}$$

The output voltage of boost part is given as follows:

$$v_{C1}(t) = v_{\text{iac}-1}(t)\frac{\frac{1-D}{jL_1\omega}}{\frac{1}{Z_{bb}}+jC_1\omega+\frac{(1-D)^2}{jL_1\omega}}. \tag{21}$$

The output voltage of buck–boost part is given as follows:

$$v_{C2}(t) = v_{C1}(t)\frac{\frac{D(1-D)}{jL_2\omega}}{\frac{1}{Z_f}+jC_2\omega+\frac{(1-D)^2}{jL_2\omega}}. \tag{22}$$

The inductor current (L_2) of buck–boost part is given as follows:

$$i_{L2}(t) = \frac{Dv_{C1}(t)-(1-D)v_{C2}(t)}{jL_2\omega}. \tag{23}$$

The output voltage of flyback part is given as follows:

$$v_{C3}(t) = V_{C2}(t)\frac{\frac{D(1-D)}{jL_3\omega}}{a\left(\frac{1}{a^2R}+j\frac{C_3\omega}{a^2}\right)+\frac{a(1-D)^2}{jL_3\omega}}. \tag{24}$$

The inductor current (L_3) of flyback part is given as follows:

$$i_{L3}(t) = \frac{DV_{C2}(t)-(1-D)av_{C3}(t)}{jL_3\omega}. \tag{25}$$

Finally, the first component of output ac current (double line frequency ripple) of the LED is obtained as follows:

$$i_O(t) = \frac{v_{C3}(t)}{R}. \tag{26}$$

As (24) shows, the amplitude of vC3(t) depends on C1, C2, and C3. The higher value of C1, C2, and C_3 causes lower ripple in v_{C3}. As seen in (14)–(26) by applying three stages in the proposed LED driver, which each stage uses a small capacitor, the ac component (ripples) of the output voltage and load current is decreased.

From (15), it is clear that $v_i(t)$ is combined of dc and ac components. The fundamental frequency in this voltage is two times of the line frequency ($2f$). Then, from sixth and seventh rows of (4), the instantaneous value of duty cycle is obtained as follows:

$$D(t) = D + d_m \sin(2\omega t) \tag{27}$$

where D and d_m are the dc component and the amplitude of the fundamental ac component, respectively.

IV. Nonlinear Control of the Proposed LED Driver Based on Input–Output Linearization

In this section, dynamic nonlinear model of the proposed LED driver is derived from (1)–(3), and then it is used to design a nonlinear controller by using IOFL [22], [23]. The nonlinear controller must be able to control the output current and the input power factor simultaneously by modulating the duty cycle. The designed control scheme consists of inner and outer loops. The inner loop is to control the inductor current i_{L1} (input power factor), and the outer loop is to control the output current i_o. These two loops are thoroughly described in the following sections.

A. Design of Nonlinear Controller of Inner Loop

With reordering (1)–(3), the state equations are rewritten as follows:

$$x' = f(x) + g(x)\,u \tag{28}$$

$$y = h(x) \tag{29}$$

where $f(x)$, $g(x)$, and u are obtained as follows:

$$f(x) = \begin{bmatrix} -\frac{1}{L_1}x_4 + \frac{1}{L_1}v_i \\ -\frac{1}{L_2}x_5 \\ \frac{N_1}{N_2 L_3}x_6 \\ \frac{1}{C_1}x_1 \\ \frac{1}{C_2}x_2 \\ -\frac{N_1}{N_2}\frac{1}{C_3}x_3 - \frac{1}{C_3}x_7 \\ \frac{1}{L_o}x_6 - \frac{R_{\text{LED}}}{L_o}x_7 - \frac{1}{L_o}v_{\text{th}} \end{bmatrix},$$

$$g(x) = \begin{bmatrix} \frac{1}{L_1}x_4 \\ \frac{1}{L_2}x_4 + \frac{1}{L_2}x_5 \\ -\frac{1}{L_3}x_5 - \frac{N_1}{N_2}\frac{1}{L_3}x_6 \\ -\frac{1}{C_1}x_1 - \frac{1}{C_1}x_2 \\ -\frac{1}{C_2}x_2 - \frac{1}{C_2}x_3 \\ \frac{N_1}{N_2}\frac{1}{C_3} \\ 0 \end{bmatrix} \tag{30}$$

$$u = D. \tag{31}$$

As mentioned above, the purpose of the first loop in the controller is to control the current of L_1 (i_{L1}) and correct the power factor. Therefore, $y = x_1$ and $\psi_1(x) = h(x) = y$. The relative degree of the output in the inner loop is $r = 1$. In order to design the inner loop, a new coordinate should be defined as follows:

$$Z = T(x) = \begin{bmatrix} h(x) \\ x_2 \\ x_3 \\ x_4 \\ x_5 \\ x_6 \\ x_7 \end{bmatrix} = \begin{bmatrix} \xi_1 \\ \eta_1 \\ \eta_2 \\ \eta_3 \\ \eta_4 \\ \eta_5 \\ \eta_6 \end{bmatrix} \tag{32}$$

where $\xi'_1 = x'_1 = \frac{-1}{L_1}x_4 + \frac{1}{L_1}(x_4 + V_i)u$

$$\eta' = \begin{bmatrix} \eta'_1 \\ \eta'_2 \\ \eta'_3 \\ \eta'_4 \\ \eta'_5 \\ \eta'_6 \end{bmatrix} = \begin{bmatrix} -\frac{1}{L_2}x_5 + \left(\frac{1}{L_2}(x_4 + V_i) + \frac{1}{L_2}x_5\right)u \\ \frac{N_1}{N_2 L_3}x_6 - \left(\frac{1}{L_3}x_5 + \frac{N_1}{N_2 L_3}x_6\right)u \\ \frac{1}{C_1}x_1 - \left(\frac{1}{C_1}x_1 + \frac{1}{C_1}x_2\right)u \\ \frac{1}{C_2}x_2 + \left(-\frac{1}{C_2}x_2 + \frac{1}{C_2}x_3 + \frac{N_2}{N_1}\frac{V_{\text{th}}}{R_{\text{LED}}}\right)u \\ -\frac{N_1}{N_2}\frac{1}{C_3}x_3 - \frac{1}{C_3}x_7 + \frac{N_1}{N_2}\frac{1}{C_3}x_3 u \\ \frac{1}{L_o}x_6 - \frac{R_{\text{LED}}}{L_o}x_7 \end{bmatrix}. \tag{33}$$

In (32), ξ_1 is used to define the control law, and η is zero dynamics. In IOFL, η' must be asymptotically stable at the point that is indicated by the following expressions, in this case, the system is called minimum phase

$$\mathrm{Z}^* = \left\{x \in R^7_{|_{\xi_1=0}}\right\}, \quad u(x) = \mathrm{u}^*(x) = -\frac{\xi'_1 \mathrm{f}(\mathrm{x})}{\xi'_1 \mathrm{g}(\mathrm{x})}|_{|_{x=Z^*}}. \tag{34}$$

Referring to (34), the value of u is obtained zero. By substituting $u = 0$ in (33), η' is obtained as follows:

$$\eta' = \begin{bmatrix} \eta'_1 \\ \eta'_2 \\ \eta'_3 \\ \eta'_4 \\ \eta'_5 \\ \eta'_6 \end{bmatrix} = \begin{bmatrix} -\frac{1}{L_2}x_5 \\ \frac{N_1}{N_2 L_3}x_6 \\ \frac{1}{C_1}x_1 \\ \frac{1}{C_2}x_2 \\ -\frac{N_1}{N_2}\frac{1}{C_3}x_3 - \frac{1}{C_3}x_7 \\ \frac{1}{L_o}x_6 - \frac{R_{\text{LED}}}{L_o}x_7 \end{bmatrix}. \tag{35}$$

As seen in (35), η' is stable and minimum phase.

A linear controller must be designed using the pole placement method to ensure that ξ_1 reaches the desired value of Y_r. New control inputs are given as follows:

$$e_1 = \xi_1 - Y_r \;\Rightarrow\; e'_1 = \xi'_1 - Y'_1 = V_1 = k_1 e_1. \tag{36}$$

By substituting ξ'_1 in (36), this equation can be rewritten as

$$V_1 = \frac{-1}{L_1}x_4 + \frac{1}{L_1}(x_4 + V_i)u \;\Rightarrow\; u = \frac{L_1 V_1 + x_4}{x_4 + V_i} \tag{37}$$

where V_1 is the control law in inner loop. To design a stable controller and ensure left-side poles, the coefficient k_1 must be negative.

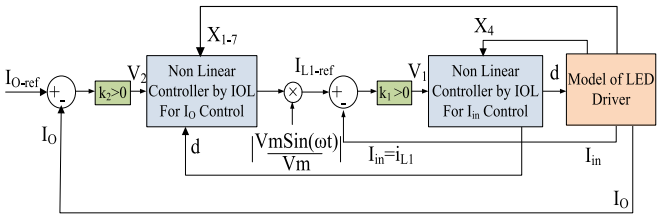

Fig. 10. Proposed driver control diagram to control the output current and power factor with nonlinear control using output–input linearization method.

B. Design of Nonlinear Controller of Outer Loop

If the inner loop correctly responds, e_1 and V_1 will be zero and $x_1 = x_{1\text{ref}}$. Referring to (31), the value of u in inner loop is obtained as follows:

$$u = \frac{x_4}{x_4 + V_i} = D. \tag{38}$$

Equation (29) is rewritten as follows:

$$f(x) = \begin{bmatrix} \frac{D-1}{L_1}x_4 + \frac{D}{L_1}V_i \\ \frac{D}{L_2}x_4 + \frac{D-1}{L_2}x_5 + \frac{D}{L_2}V_i \\ -\frac{D}{L_2}x_5 + \frac{N_1(D-1)}{N_2 L_3}x_6 \\ -\frac{D}{C_1}x_2 \\ \frac{1-D}{C_2}x_2 + \frac{D}{C_2}x_3 + \frac{N_2}{N_1}\frac{DV_{\text{th}}}{R_{\text{LED}}} \\ \frac{N_1}{N_2}\frac{D-1}{C_3}x_3 - \frac{1}{C_3}x_7 \\ \frac{1}{L_o}x_6 - \frac{R_{\text{LED}}}{L_o}x_7 \end{bmatrix}, \quad g(x) = \begin{bmatrix} 0 \\ 0 \\ 0 \\ -\frac{1}{C_1}D + \frac{1}{C_1} \\ 0 \\ 0 \\ 0 \end{bmatrix} \tag{39}$$

where d in the inner loop is obtained from (38). As stated before, the purpose of the outer loop is to obtain the desired i_{L1}, where this current is the input of the controller that is written as

$$u = x_1. \tag{40}$$

However, the purpose of the outer control loop is to control i_o, the fallowing equation is assumed, $\psi_1(x) = h(x) = y = x_7$. The relative degree of the output in the outer loop is $r = 6$. The controller input u is obtained as

$$u = \frac{1}{\frac{\partial \Psi_6}{\partial x} g(x)} \left[-\frac{\partial \Psi_6}{\partial x} f(x) + V_2 \right] \tag{41}$$

where V_2 is the control law that is obtained as follows:

$$V_2 = k_2 e_2 = k_2 (Y_2 - Y_{2\text{ref}}). \tag{42}$$

To preserve stability, the coefficient k_2 must be negative.

The block diagram of the nonlinear controller with the input–output linearization method is shown in Fig. 10. This figure shows how the duty cycle can be controlled by input–output linearization to obtain the desired output current and high-power factor. In the proposed driver, the controller coefficients are $k_1 = -10$ and $k_2 = -10^{27}$.

V. Comparison With the Prior-Art LED Drivers

In this section, the proposed LED driver is compared with the state-of-the-art LED drivers and two PFC converters. To this end, the LED drivers in [19], [21], [24], and [25] and PFC converters in [26] and [27] are taken into consideration to be compared with the proposed LED driver. Different electrical parameters and required components of the considered LED drivers and PFC converters along with the proposed one are listed in Table II. One of the vulnerable components in power electronic converters, especially LED drivers, is electrolyte capacitors. Since this component has high failure rate, they can remarkably reduce the reliability and lifetime of power electronic converters, including LED drivers. Hence, eliminating this component and replacing it with ceramic/polyester capacitors (with low capacity) can tackle the problem. Referring to Table II, it is seen that, due to using three dc–dc stages, the proposed LED driver and PFC in [27] do not need any electrolyte capacitor. This can be count as one of the main advantages of the proposed LED driver compared with the other considered LED drivers. It worth mentioning that the PFC in [27] succeeded to eliminate the electrolyte capacitor by both integrating two converting stages and increasing the switching frequency; this in turn caused increasing in power losses and using costly high-frequency semiconductors. The other advantage of the proposed and the LED drivers in [19], [21], and [25] and PFC in [27] is using only one active switch. This can reduce the complexity and cost.

Furthermore, to avoid light flicker, the LED drivers are required to reduce the output current ripple as much as possible; in this regard, the proposed LED driver can provide an output current with current ripple lower than 15% that meet the related standards [6]. This parameter is 5% and 10% for the articles presented in [21] and [25], respectively. The LED drivers in the mentioned references achieve lower ripple with expense of using large electrolyte capacitors. The mentioned parameter is high in the other LED driver, as listed in Table II.

Output current ripple in the PFCs in [26] and [27] is 4% and 5%, respectively. It is to be noted that the performance of the mentioned PFCs is not investigated in the present of LED load. Owing to the fact that LEDs have a nonlinear *V–I* characteristic [referring to Fig. 1(b)], the current ripple of the PFCs in the mentioned references is not clear and can be critical.

However, the ON-grid LED drivers are supplied through ac grid, and they should be able to correct power factor. As seen in Table II, the proposed LED driver can satisfactorily correct power factor. What is more, in the case of total harmonic distortion (THD) and efficiency, the proposed LED driver can overtake the other considered LED drivers and PFCs.

VI. Simulation and Experimental Verification

A 145-W prototype of the proposed LED driver, which is supplied by 110 Vrms/50 Hz ac voltage, is employed to extract

TABLE II
COMPARISON OF THE CONSIDERED LED DRIVERS

LED driver	[19]	[21]	[24]	[25]	[26]	[27]	Proposed Structure
Utilized Component				**Number**			
Diode	4	5	6	6	1	3	5
Switch	1	1	2	1	2	1	1
Rectifier bridge	1	1	-	1	1	1	1
Inductor	1	2	2	3	1	2	2
Electrolyte Capacitor	1	2	2	2	2	Not needed	Not needed
Polyester Capacitor	1	3	1	2	0	2	3
Stages in integrated structure	2	2	2	2	1	2	3
Transformer	1	2	-	1	1	-	1
Parameters				**Values**			
Power Factor	>0.97	>0.995	>0.99	>0.985	>0.99	>0.995	>0.995
THD (%)	<22.3	<10	<10.9	<9	<7	<3.5	<10
Output current ripple (%)	46	5	20	10	4	5	15
Nominal Output Power (W)	104	100	42	100	100	100	143.6
Total capacitor size (μF)	78.1	267.171	170.8	301.84	377	35	19.4
Efficiency range (%) @ P [W] , f_s (kHz)	92.5 @90 ,100	92@100 , 100	96.4@ 42 ,50	91.5@100 , 100	93.2@80 , 300	89.5@100 , 80	97@ 143 ,33

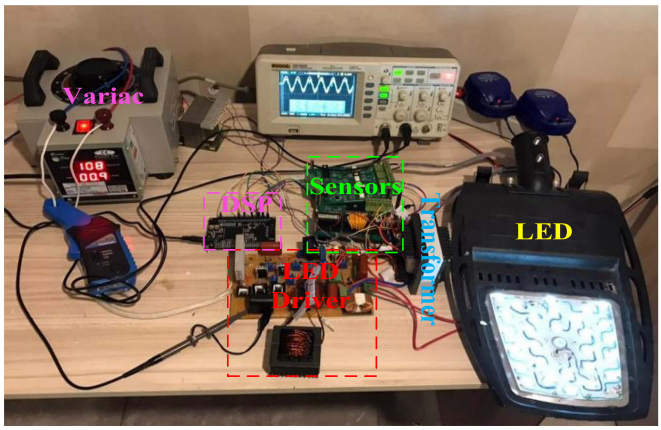

Fig. 11. Prototype of the proposed LED driver.

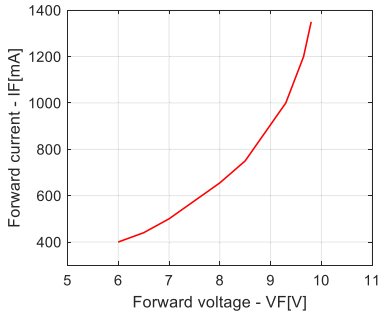

Fig. 12. Characteristic curve of 10 W Epistar chip high-power LED.

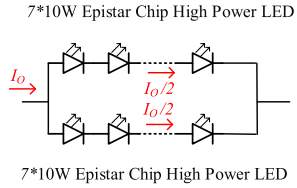

Fig. 13. LEDs connection configuration.

TABLE III
DRIVER PARAMETERS AND DEVICE TYPE

Device label	Definition
LED	14*10 W Epistar Chip High-Power LED
$D_1 - D_5$	SFF508G 5 A,600 V
Power switch	IRFP450
Bridge rectifier	D15XB 60
C_1, C_2, and C_3 (μF)	4.7, 4.7, 10
L_1, L_2 ,L_3, and L_O (mH)	0.2, 2,0.4,0.02
Transformer ratio (N1/N2)	2
L_f (Input filter)	1 mH
C_f (Input filter)	2 μF
Output power	143.6 W
Microcontroller	DSP-TMSF28335
Switching frequency	33 kHz

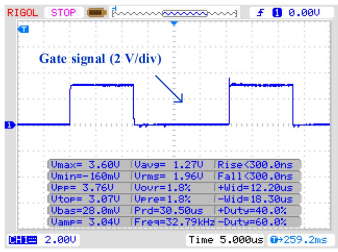

Fig. 14. Experimental result of the switch *S* gate signal.

the experimental results and verify the theoretical analysis. The prototype is exhibited in Fig. 11 and the components utilized in the prototype are listed in Table III.

In the proposed driver, 14 number of 10 W Epistar Chip High-Power LEDs with the forward current and forward voltage characteristics, as shown in Fig. 12, are connected to the output terminal. The LEDs are connected in two parallel strings, where each strings includes seven LEDs in series, as shown in Fig. 13.

The ON-state voltage and resistance of each LED are 0.8 V and 3 Ω, respectively. Then, $V_{\rm th}$ and $R_{\rm LED}$ in model of driver in Fig. 5 are 5.6 V and 21 Ω, accordingly.

The gate signal of the active switch is shown in Fig. 14. As seen in this figure, the switching frequency of the proposed driver is 33 kHz.

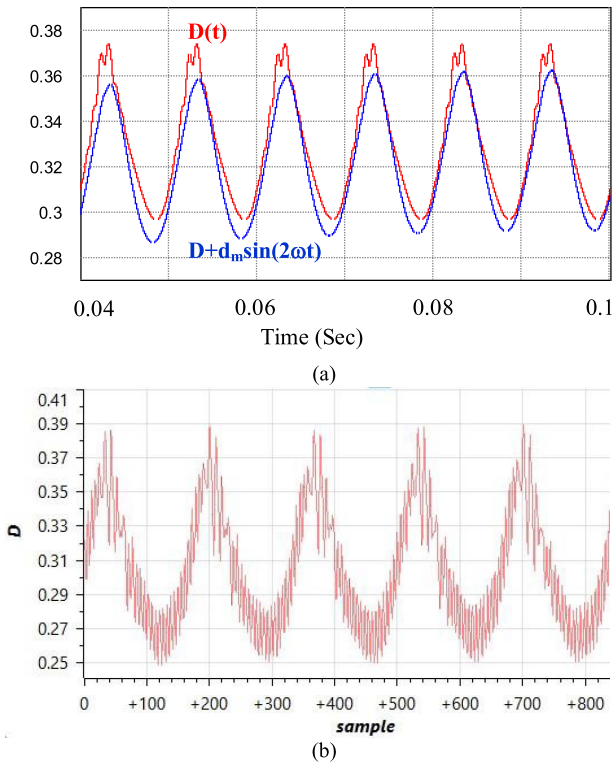

Fig. 15. Duty cycle using IOFL controller. (a) Summation results of the average (D) and fundamental component ($d_m\text{Sin}(2\omega t)$) together with the entire duty cycle ($D(t)$) in simulation. (b) Experimental result of entire duty cycle (with sampling frequency of 17 kHz).

The simulation results of the duty cycle using IOFL nonlinear controller are figured out and shown in Fig. 15(a). In this figure, the red curve shows the entire duty cycle ($D(t)$), and the blue curve shows the summation of the average (D) and fundamental component ($d_m\text{Sin}(2\omega t)$) of the $D(t)$. Additionally, the experimental duty cycle, as plotted in Code Composer Studio software, is shown in Fig. 15(b).

Fig. 16 shows the simulation and experimental results of the input current, voltage, and instantaneous power. As seen in this figure, the input current and voltage are sinusoidal and in phase. The current and voltage waveforms along with the shown instantaneous power, which has no negative value (with the average of 147 W), ensure that the proposed driver has succeeded to provide unity power factor.

In order to investigate the ac-side current qualification, the fast Fourier transform (FFT) analysis is depicted in Fig. 17. Considering that the fundamental frequency is 50 Hz, as observed, the 3th, 5th, 7th, 9th, 11th, and 13th current harmonic orders are 0.12 A, 0.06 A, 0.02 A, 0.01 A, 0.01 A, and 0.005 A, respectively. Taken the mentioned values into account, the THD of the input current is 9.6%.

The LED drivers are required to meet IEC 61000-3-2 Class C standard [5]; in order to assess the THD of the proposed LED driver, the percentage of prominent current harmonic orders is recorded and compared with the standard values. The result is depicted in Fig. 18. As seen in this figure, the recorded harmonic

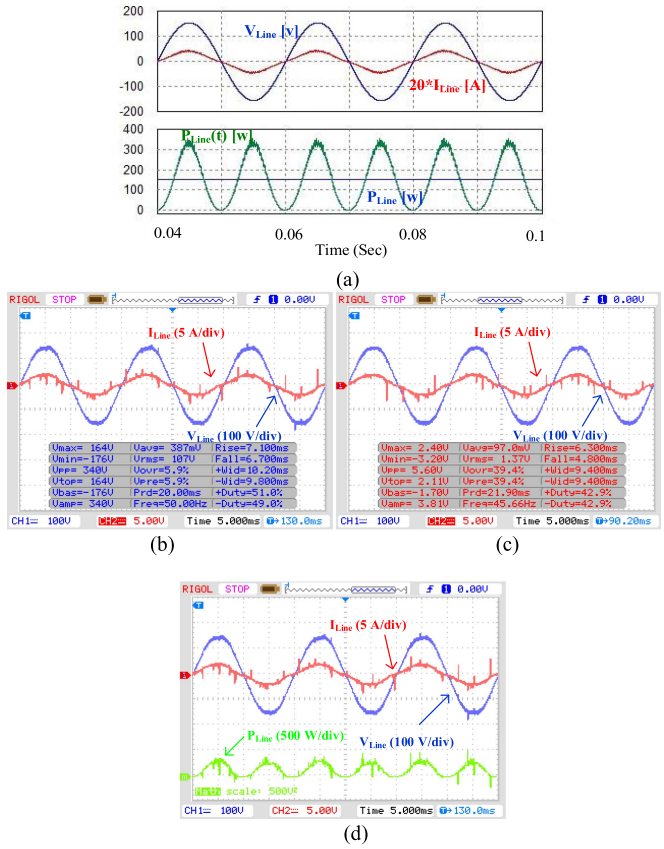

Fig. 16. Simulation and experimental results of different parameters at the ac side. (a) Simulation results of voltage, current, and instantaneous and average power. (b) Experimental results of voltage and current showing voltage measurements. (c) Experimental results of voltage and current showing current measurements. (d) Experimental results of voltage, current, and instantaneous power.

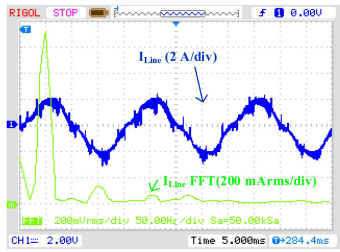

Fig. 17. Experimental results of AC-side current and its FFT analysis.

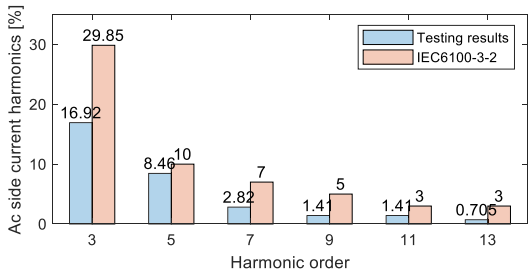

Fig. 18. Comparison result of the AC-side current harmonics with that of the IEC 61000-3-2 class C standard.

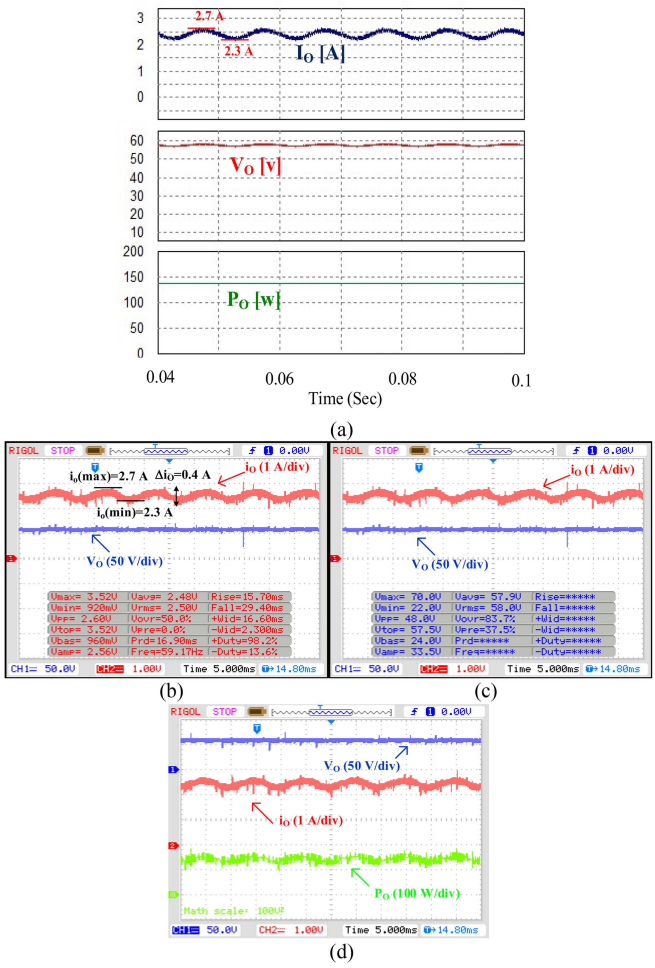

Fig. 19. Simulation and experimental results of different parameters at the output terminal. (a) Simulation results of voltage, current, and power. (b) Experimental results of voltage and current showing current measurements. (c) Experimental results of voltage and current showing voltage measurements. (d) Experimental results of voltage, current, and power.

values of the proposed driver are satisfactorily lower than the standard values.

The simulation and experimental results of the output current, voltage across the LED string, and output power are exhibited in Fig. 19. As seen in these figures, and referring to Fig. 16(d), the values of the input and output powers are 147 W and 143.6 W, respectively, this means the efficiency of driver is 97.6%. Furthermore, as it is observed in Fig. 19, the ripple of the output current is insignificant. This indicates that the flicker of the LED light is negligible.

The recommended operation area of LEDs according to "IEEE recommended practices for modulating current in high-brightness LEDs for mitigating health risks to viewers" [6] is depicted in Fig. 20. LEDs operating in the mentioned area would have an acceptable luminance flicker. According to the article presented in [6], the current modulation is obtained as follows:

$$\text{Mod}\% = \frac{i_{o(\max)} - i_{o(\min)}}{i_{o(\max)} + i_{o(\min)i}} \times 100. \tag{43}$$

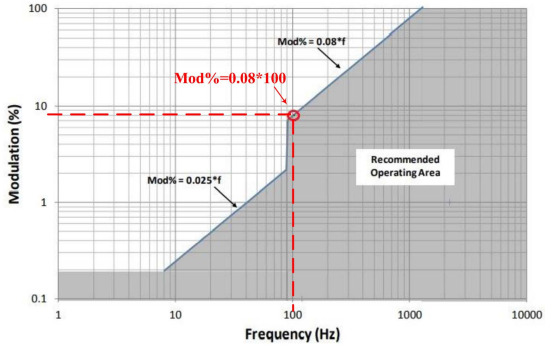

Fig. 20. Recommended operating area as a function of frequency and modulation (%) [6].

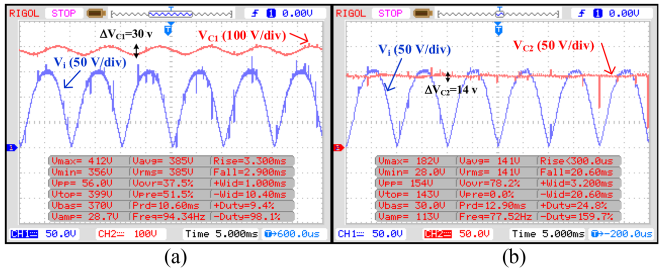

Fig. 21. Experimental results of rectifier output voltage (V_i) and capacitors' voltages of (a) C_1 and (b) C_2.

By constituting the upper and lower values of the output current in Fig. 19(a) and (b), which are, respectively, 2.7 A and 2.3 A, in (43), the Mod is obtained 8%. Referring to Fig. 20, for the ripple frequency of 100 Hz, this value is in an acceptable area.

The output voltage of rectifier (V_i) and capacitors' voltages are exhibited in Fig. 21. Referring to this figure, it is obvious that the voltage ripple of C_2 is lower than the voltage ripple of C_1. It means that the higher the number of stages in driver is, the lower is the voltage ripple of the final stage. Therefore, the output voltage ripple decreases causing the output current to decrease significantly.

The output voltage of rectifier (V_i) and inductors' currents are exhibited in Fig. 22. Referring to this figure, it is seen that the current of inductor L_1 reaches zero when the value of the input voltage (V_i) is zero. This can again emphasis the capability of the proposed LED driver to provide a unity power factor.

It was impossible to validate the theoretical analysis, which was obtained under an ascertained duty cycle in Section III, through the above results because these results are obtained by using IOFL nonlinear controller under variating duty cycle. To the end of validating the theoretical analysis of the voltage and current ripples under noncontrolled condition, which are indicated in (21), (22), (24), and (26), we resorted to simulation results. The voltage and current ripples are obtained by using the parameters, as listed in Table III. The voltage ripple of the utilized capacitors is shown in Fig. 23(a). Comparing the ripple values shown in this figure by the theoretical analysis [(21),

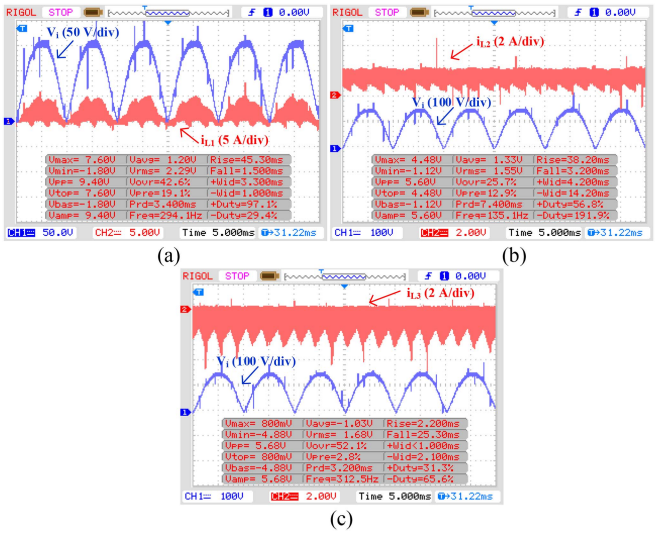

Fig. 22. Experimental results of rectifier output voltage (V_i) and inductors' currents of (a) L_1, (b) L_2, and (c) L_3.

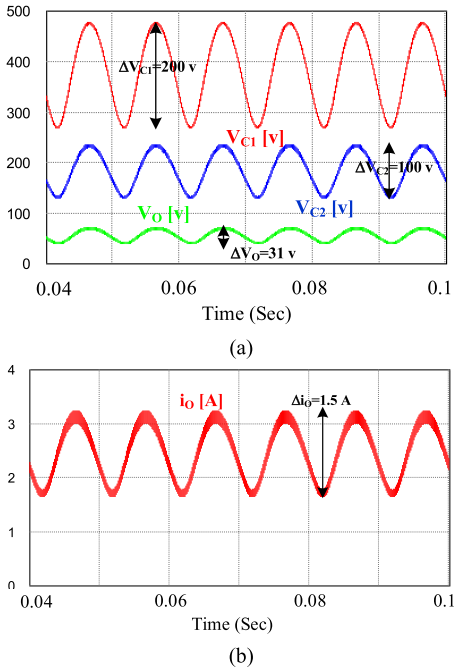

Fig. 23. Simulation results with ascertained duty cycle, (a) voltage of capacitors, and (b) output current.

(22), and (24)], it is seen that the voltage ripple obtained by the theoretical analysis is in accordance with the ripples obtained by the simulation results. These are also the case for the output current (26) which is shown in Fig. 23(b). In conclusion, as shown in Fig. 23(a), the voltage ripple is reduced in each stage. In addition, as implied by the experimental results, using a controlled duty cycle helps to decrease the ripples as much as possible.

The primary and secondary voltages of the flyback transformer are demonstrated in Fig. 24. Because the transformer

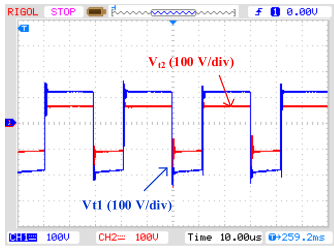

Fig. 24. Experimental results of input and output voltage of flyback transformer.

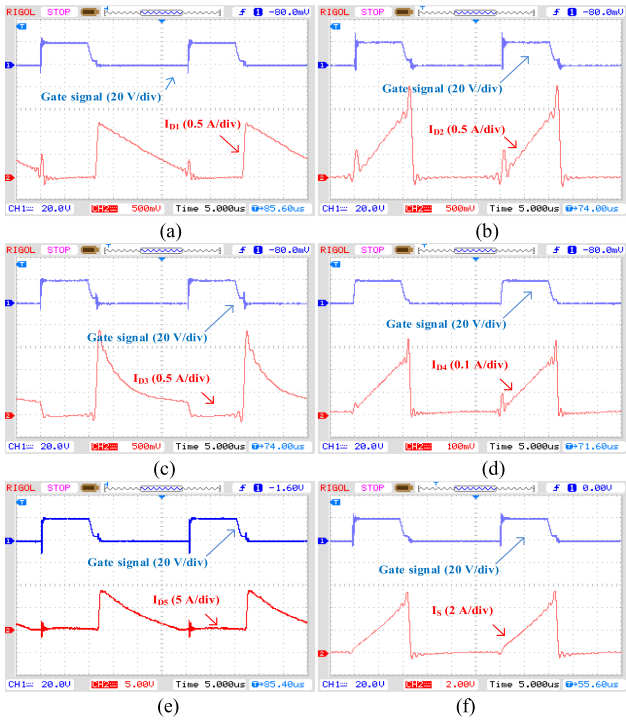

Fig. 25. Experimental results showing current stresses. (a) Gate signal of the switch S and current of D_1. (b) Gate signal of the switch S and current of D_2. (c) Gate signal of the switch S and current of D_3. (d) Gate signal of the switch S and current of D_4. (e) Gate signal of the switch S and current of D_5. (f) Gate signal of the switch S and current of S.

ratio of the transformer is 2, the primary voltage is two times higher than the voltage at the secondary side.

One of the most important parameters in any power electronics' devices is the current stress of the utilized semiconductors. In order to scrutinize the mentioned parameter in the proposed LED driver, the current stresses of all the employed semiconductors along with the exerted gate signal of the active switch (S) are indicated in Fig. 25. According to these figures, D_5 and D_4 tolerate the highest and lowest current stress, respectively, also the only one utilized switch S tolerates 5 A.

In order to investigate the dynamic performance of the proposed LED driver, it is considered that the LED driver normally supplies one LED string, including seven series-connected LEDs. Then, the second string with the same characteristics is connected in parallel. The results are shown in Fig. 26. As it is

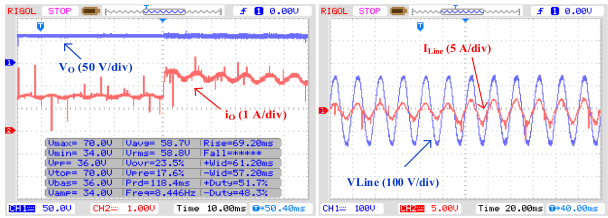

(a) (b)

Fig. 26. Experimental results of dynamic performance. (a) Output voltage and current. (b) Input voltage and current.

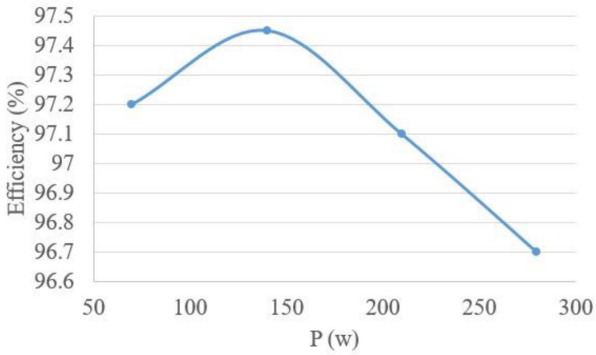

Fig. 27. Experimental efficiency.

seen in Fig. 26(a), the current ripple increases when the second string is added. Obviously, the input current would increase as the second string is added to the output, as seen in Fig. 26(b).

By connecting four configurations of LEDs with different consuming powers at the output terminal of the prototype, the efficiency is figured out and shown in Fig. 27.

VII. Conclusion

In this article, a new isolated LED driver was put forth. This LED driver is synthetized with three integrated dc–dc converters (boost, buck–boost, and flyback) to approach the following features:

PFC capability;

low output current ripple;

eliminating electrolyte capacitor;

using only one switch for three integrated dc–dc converters;

eradicating parasitic inductor power losses of the flyback transformer.

In order to reach fast response, a nonlinear IOFL was designed for the proposed LED driver. The performance of the proposed LED driver and designed nonlinear controlling approach was analyzed and verified through simulation and experimental results. The provided results validated the versatility and feasibility of the proposed LED driver and designed control approach.

Acknowledgment

The authors would like to thank Dr. H. K. Jahan for his valuable and constructive suggestions during the planning and development of this article. His willingness to give his time so generously has been highly appreciated.

References

[1] Y. Wang, J. M. Alonso, and X. Ruan, "A review of LED drivers and related technologies," *IEEE Trans. Ind. Electron.,* vol. 64, no. 7, pp. 5754–5765, Jul. 2017.

[2] M. Arias, A. Vázquez, and J. Sebastián, "An overview of the AC-DC and DC-DC converters for LED lighting applications," *Automatika*, vol. 53, no. 2, pp. 156–172, 2012.

[3] I. Castro, A. Vazquez, M. Arias, D. G. Lamar, M. M. Hernando, and J. Sebastian, "A review on flicker-free AC–DC LED drivers for single-phase and three-phase AC power grids," *IEEE Trans. Power Electron.,* vol. 34, no. 10, pp. 10035–10057, Oct. 2019.

[4] S. Salehahari, E. Babaei, and M. Sarhangzadeh, "A new structure of multilevel inverters based on coupled inductors to increase the output current," in *Proc. 6th Power Electron., Drive Syst. Technol. Conf.*, 2015, pp. 19–24.

[5] I.E.Commission, "Electromagnetic compatibility (EMC)—Part 3-2: Limits—Limits for harmonic current emissions (equipment input current≤ 16 A per phase)," Int. Electrotech. Commission (IEC), Geneva, Switzerland, 2018.

[6] "IEEE recommended practices for modulating current in high-brightness LEDs for mitigating health risks to viewers," *IEEE Std 1789-2015*, pp. 1–80, Jun. 5, 2015, doi: 10.1109/IEEESTD.2015.7118618.

[7] G. Z. Abdelmessih, J. M. Alonso, N. D. S. Spode, and M. A. Dalla Costa, "Electrolytic-capacitor-less off-line LED driver based on integrated parallel buck-boost and boost converter," in *Proc. IEEE Ind. Appl. Soc. Annu. Meeting*, 2020, pp. 1–7.

[8] A. Bagheran and M. R. Yazdani, "An isolated PFC zeta-forward single-stage single-switch for LED driver without electrolytic capacitor," *Electr. Power Compon. Syst.,* vol. 48, no. 6/7, pp. 682–696, 2020.

[9] J. Zeng, F. Liu, J. Liu, and K. W. E. Cheng, "A flexible mode electrolytic capacitor-free LED driver with high efficiency over a wide range of input voltage," *IEEE Trans. Power Electron.,* vol. 35, no. 8, pp. 8490–8500, Aug. 2020.

[10] S. Wang, X. Ruan, K. Yao, S.-C. Tan, Y. Yang, and Z. Ye, "A flicker-free electrolytic capacitor-less AC–DC LED driver," *IEEE Trans. Power Electron.*, vol. 27, no. 11, pp. 4540–4548, Nov. 2012.

[11] D. Camponogara, D. R. Vargas, M. A. Dalla Costa, J. M. Alonso, J. Garcia, and T. Marchesan, "Capacitance reduction with an optimized converter connection applied to LED drivers," *IEEE Trans. Ind. Electron.,* vol. 62, no. 1, pp. 184–192, Jan. 2015.

[12] M. Khatua et al., "High-performance megahertz-frequency resonant DC–DC converter for automotive LED driver applications," *IEEE Trans. Power Electron.*, vol. 35, no. 10, pp. 10396–10412, Oct. 2020.

[13] Y. Wang, Y. Guan, D. Xu, and W. Wang, "A CLCL resonant DC/DC converter for two-stage LED driver system," *IEEE Trans. Ind. Electron.,* vol. 63, no. 5, pp. 2883–2891, May 2016.

[14] X. Liu, X. Li, Q. Zhou, and J. Xu, "Flicker-free single switch multi-string LED driver with high power factor and current balancing," *IEEE Trans. Power Electron.,* vol. 34, no. 7, pp. 6747–6759, Jul. 2019.

[15] F. Pouladi, H. Farzanehfard, E. Adib, and H. L. Sage, "Single-switch soft-switching LED driver suitable for battery-operated systems," *IEEE Trans. Ind. Electron.,* vol. 66, no. 4, pp. 2726–2734, Apr. 2019.

[16] H. Wu, S.-C. Wong, and C. K. Tse, "A more efficient PFC single-coupled-inductor multiple-output electrolytic capacitor-less LED driver with energy-flow-path optimization," *IEEE Trans. Power Electron.,* vol. 34, no. 9, pp. 9052–9066, Sep. 2019.

[17] H. Wu, S.-C. Wong, C. K. Tse, and Q. Chen, "A PFC single-coupled-inductor multiple-output LED driver without electrolytic capacitor," *IEEE Trans. Power Electron.,* vol. 34, no. 2, pp. 1709–1725, Feb. 2019.

[18] C. Gobbato, S. V. Kohler, I. H. de Souza, G. W. Denardin, and J. de Pelegrini Lopes, "Integrated topology of DC–DC converter for LED street lighting system based on modular drivers," *IEEE Trans. Ind. Appl.,* vol. 54, no. 4, pp. 3881–3889, Jul./Aug. 2018.

[19] G. G. Pereira, M. A. Dalla Costa, J. M. Alonso, M. F. De Melo, and C. H. Barriquello, "LED driver based on input current shaper without electrolytic capacitor," *IEEE Trans. Ind. Electron.,* vol. 64, no. 6, pp. 4520–4529, Jun. 2017.

[20] F. Wang, L. Li, Y. Zhong, and X. Shu, "Flyback-based three-port topologies for electrolytic capacitor-less LED drivers," *IEEE Trans. Ind. Electron.,* vol. 64, no. 7, pp. 5818–5827, Jul. 2017.

[21] S. Zhang, X. Liu, Y. Guan, Y. Yao, and J. M. Alonso, "Modified zero-voltage-switching single-stage LED driver based on class E converter with constant frequency control method," *IET Power Electron.,* vol. 11, no. 12, pp. 2010–2018, 2018.
[22] M. Sarhangzadeh, S. H. Hosseini, M. B. B. Sharifian, and G. B. Gharehpetian, "Multiinput direct DC–AC converter with high-frequency link for clean power-generation systems," *IEEE Trans. Power Electron.*, vol. 26, no. 6, pp. 1777–1789, Jun. 2011.
[23] M. Sarhangzadeh, S. H. Hosseini, M. B. B. Sharifian, G. B. Gharehpetian, and O. Sarhangzadeh, "Dynamic analysis of DVR implementation based on nonlinear control by IOFL," in *Proc. 24th Can. Conf. Elect. Comput. Eng.*, 2011, pp. 264–269.
[24] A. Malschitzky, E. Agostini, and C. B. Nascimento, "Integrated bridgeless-boost nonresonant half-bridge converter employing hybrid modulation strategy for LED driver applications," *IEEE Trans. Ind. Electron.,* vol. 68, no. 9, pp. 8049–8060, Sep. 2021.
[25] Y. Wang, J. Huang, W. Wang, and D. Xu, "A single-stage single-switch LED driver based on class-E converter," *IEEE Trans. Ind. Appl.,* vol. 52, no. 3, pp. 2618–2626, May/Jun. 2016.
[26] H. Li, S. Li, W. Xiao, and S. Y. R. Hui, "A modulation method for capacitance reduction in active-clamp flyback-based AC–DC adapters," *IEEE Trans. Power Electron.,* vol. 37, no. 8, pp. 9455–9467, Aug. 2022.
[27] S. Li, W. Qi, J. Wu, S.-C. Tan, and S.-Y. Hui, "Minimum active switch requirements for single-phase PFC rectifiers without electrolytic capacitors," *IEEE Trans. Power Electron.,* vol. 34, no. 6, pp. 5524–5536, Jun. 2019.

Behnam Vakili received the B.Sc. and M.Sc. degrees in electrical engineering from Tabriz Branch, Islamic Azad University, Tabriz, Iran, in 2013 and 2015, respectively. He is currently working toward the Ph.D. degree in electrical engineering with the Department of Electrical Engineering, Sanandaj Branch, Islamic Azad University, Sanandaj, Iran.

His research interests include power electronic application in renewable energy systems, three-phase motors, three-phase drivers in elevators, and LED drivers.

Mitra Sarhangzadeh received the B.Sc., M.Sc., and Ph.D. degrees in electrical engineering from the University of Tabriz, Tabriz, Iran, in 2001, 2004, and 2011, respectively.

She is an Assistant Professor with the Department of Electrical Engineering, Tabriz Branch, Islamic Azad University, Tabriz, Iran. Her research interests include power electronic application in renewable energy systems, energy management in power electronic systems, modeling and control of power electronic systems, electrified railway systems, inverters, electric vehicles, and power quality compensation systems, such as SVC, UPQC, and FACTS devices.

Arez Nostratpour received the B.Sc. degree in electronic engineering from the University of Kurdistan, Sanandaj, Iran, in 2010, the M.Sc. degree in electronics from the Islamic Azad University of Arak, Arak, Iran, in 2012, and the Ph.D. degree in the field of electronics from Science and Research Branch, Islamic Azad University, Tehran, Iran, in 2018.

He is an Assistant Professor with the Department of Electrical Engineering, Sanandaj Branch, Islamic Azad University, Sanandaj, Iran. His research interests include micro and nanoelectronics, and optoelectronics.

Jaber Fallah Ardashir received the B.Sc., M.Sc., and Ph.D. degrees in electrical engineering from the Department of Electrical Engineering, Azerbaijan Shahid Madani University, Tabriz, Iran, Zanjan University, Zanjan, Iran, and Tabriz University, Tabriz, Iran, in 2010, 2012, and 2017, respectively.

He was a Visiting Ph.D. Scholar with the Department of Energy, Aalborg University, Aalborg, Denmark, from 2015 to 2016. He is currently an Assistant Professor of electrical power engineering with the Department of Electrical Engineering, Tabriz Branch, Islamic Azad University, Tabriz, Iran. His research interests lie in the fields of power electronic converters, renewable energy systems, and reliability.